Core-valence-separated coupled-cluster-singles-and-doubles complex-polarization-propagator approach to X-ray spectroscopies

Faber, Rasmus; Coriani, Sonia

Published in:
Physical Chemistry Chemical Physics

Link to article, DOI:
10.1039/c9cp03696b

Publication date:
2020

Document Version
Peer reviewed version

PCCP

ROYAL SOCIETY OF CHEMISTRY

ARTICLE TYPE

Cite this: DOI: 10.1039/xxxxxxxxxx

Core-valence-separated coupled-cluster-singles-and-doubles complex-polarization-propagator approach to x-ray spectroscopies

Rasmus Faber,*[a] and Sonia Coriani*[a]

Received Date
Accepted Date

DOI: 10.1039/xxxxxxxxxx

www.rsc.org/journalname

The iterative subspace algorithm to solve the complex linear response equation of damped coupled cluster response theory presented, up to CCSD level, by Kauczor *et al., J. Chem. Phys.*, 2013 **139**, 211102, and recently extended to the solution of the complex left response multipliers by Faber and Coriani, *J. Chem. Theory Comput.*, 2019 **15**, 520, has been modified as to include a core-valence separation projection step in the iterative procedure. This allows to overcome serious convergence issues that specifically manifest themselves at the CCSD level when addressing core-related spectroscopic effects using large basis sets. The spectra obtained adopting the new scheme for x-ray absorption and circular dichroism, as well as Resonant Inelastic-X-ray Scattering, are presented and discussed. Core-valence separated results for non-resonant X-ray emission are also reported.

1 Introduction

The complex-polarization-propagator (CPP) approach,[1–10] also known as damped response theory,[11] is a valuable method to tackle the computational simulation of spectroscopic effects in cases where a large density of states and/or additional resonant conditions are involved, and traditional stick-spectra-based approaches may therefore fail.

The method relies on the ability to solve linear response equations for a complex, or damped, frequency,[10] and it has been successfully implemented at various levels of electronic structure theory, including Hartree-Fock and Time-Dependent Density Functional theory,[1–3,12] as well as Multiconfigurational Self-Consistent Field,[1,2] Algebraic Diagrammatic Construction (ADC)[13] and Coupled-Cluster (CC) Theory.[7–9,14] Extensions to solvated environments[15,16] and in the relativistic domain[17] have also been presented. Applications encompass the calculation of linear absorption spectra in different frequency regions, including X-ray absorption spectra,[4,5,8,14] electronic circular dichroism spectra,[18] magnetic-field and nuclear-spin induced circular dichroism,[19–21] magneto-chiral dichroism and birefringence dispersion,[22] two-photon absorption in both UV-vis and X-ray regimes,[6,23] Cauchy coefficients at imaginary frequency,[7,13,24] and, more recently, Resonant Inelastic X-ray Scattering.[9,25]

At the CC level, two different algorithms have been proposed to obtain complex response functions. In the first one,[7,8] a diagonal basis of eigenvectors was generated by diagonalization of an approximate Lanczos-based tridiagonal representation of the CC Jacobian, and used to construct the imaginary or real components of the complex linear response function via a sum-over-state-like expression that includes the damping parameter γ. In the second one,[9,14] the damped linear response equations yielding the complex (real and imaginary components thereof) amplitudes and multipliers were solved via a generalization of the reduced-space algorithm used in conventional CC response.

The main drawbacks of the first approach are the need to predecide the size of the truncated Lanczos basis, that prevents the *a priori* control of the convergence thresholds, and the need to store a large number of Lanczos vectors on file, resulting in disk and I/O issues for larger systems. Moreover, if the target excited states lie in the X-ray region, large Lanczos chain lengths are required to obtain converged X-ray energies, unless specific core-valence separated (CVS) techniques are adopted.[26–28]

In the CPP-CC method of Ref. 14, on the other hand, the damped response solver manifests severe convergence issues at the CC singles and doubles (CCSD) level in the high-energy frequency region and in particular when larger basis sets are used.

These issues can be rationalized as originating from the high density of doubly excited/ionized valence states that form the continuum in which the X-ray absorption bands are embedded.

[a] *DTU Chemistry - Department of Chemistry, Technical University of Denmark, Kemitorvet Building 207, DK-2800 Kongens Lyngby, Denmark. E-mail: rfaber@kemi.dtu.dk (R. Faber); soco@kemi.dtu.dk (S. Coriani)*

† Electronic Supplementary Information (ESI) available: [details of any supplementary information available should be included here]. See DOI: 10.1039/cXCP00000x/

Thus, even though the essence of the CPP method is to introduce a damping parameter γ in the (linear) response functions to specifically remove the singularities when the external frequency approaches a resonant value, in the CCSD case this damping is not sufficient to guarantee convergence as the basis set increases, due to the enormous number of closely lying double excited/ionized states that become accessible when a large basis set is used. Too many potential resonances can occur for just one parameter to take care of, and less and less diagonal the CC Jacobian becomes, which compromises the efficiency of the diagonal preconditioner that is typically used to accelerate convergence. As a further proof, in the case of the CC singles and approximate doubles method, CC2, where the double-double block of the Jacobian exactly corresponds to the orbital energy differences matrix, the damped response equations do converge.

To overcome these problems, we here propose to apply a core-valence separation projector[27] during the solution of the CCSD complex response equations, to remove the continuum of valence ionized states. The performance of the resulting CVS-CPP algorithm is illustrated by calculations, within the CCSD linear response (LR-CCSD) framework, of near-edge-absorption fine structure (NEXAFS) and X-ray circular dichroism (XCD) and, within CCSD quadratic response (QR-CCSD), of Resonant Inelastic X-ray Scattering (RIXS). CVS-CCSD results for non-resonant X-ray emission (XES), computed, according to our previously proposed recipe,[9] as transitions between valence- and core-ionized states, are also reported for completeness. Equation-of-motion (CVS-CPP-EOM-CCSD) variants of the same properties could also be derived by modifications to the property Jacobian matrix and final property expressions.[9,29,30] An alternative derivation of RIXS and XES exploiting a conceptually analogous CVS-DIIS damped solver within the frozen-core fc-CVS-EOM-CCSD framework[31] is presented in Ref. 32.

2 Theory

2.1 NEXAFS, XCD and RIXS within the CPP-(CVS)-CC formalism

NEXAFS cross-sections $\sigma(\omega)$ can be computed from the imaginary electric dipole–electric dipole linear response function[1,4,5,8]

$$\sigma_{XAS}(\omega) \propto \omega \Im \langle\langle \mu_\alpha ; \mu_\alpha \rangle\rangle_\omega^\gamma \tag{1}$$

where μ_α is the electric dipole moment, and the incident frequency is in the region of absorption of the relevant X-ray edge. XCD cross-sections, on the other hand, are obtained from the real part of the electric dipole and magnetic dipole linear response function[1,18,22]

$$\sigma_{XCD}(\omega) \propto \omega \Re \langle\langle \mu_\alpha ; m_\alpha \rangle\rangle_\omega^\gamma \tag{2}$$

(since the magnetic dipole operator m is an imaginary operator). The RIXS cross section is obtained from the transition strengths σ^{0f} averaged over all molecular orientations and over the polarization of the emitted radiation. The latter depends on the angle θ between the polarization vector of the incident photon, and the propagation vector of the scattered photon[9,25]

$$\sigma_\theta^{0f} = \frac{\omega'}{\omega}\frac{1}{15}\sum_{XY}\left[\left(2-\frac{1}{2}\sin^2\theta\right)\mathscr{F}_{XY}^{0f}(\omega)\mathscr{F}_{XY}^{f0}(\omega) + \left(\frac{3}{4}\sin^2\theta-\frac{1}{2}\right)\left(\mathscr{F}_{XY}^{0f}(\omega)\mathscr{F}_{YX}^{f0}(\omega)+\mathscr{F}_{XX}^{0f}(\omega)\mathscr{F}_{YY}^{f0}(\omega)\right)\right] . \tag{3}$$

where $\mathscr{F}_{XY}^{0f}(\omega)$ and $\mathscr{F}_{XY}^{f0}(\omega)$ are the left and right Kramers-Heisenberg- Dirac (KHD) amplitudes,[33,34] respectively. Sum-over-states expressions for the amplitudes assuming the same inverse lifetime for all states can be found in Refs. 9 and 25.

In CC damped linear response, the complex polarizability is computed according to:

$$\langle\langle X;Y\rangle\rangle_\omega^\gamma = \frac{1}{2}C^{\pm\omega}\{\eta^X t^Y(\omega+i\gamma)+\eta^Y t^X(-\omega-i\gamma)+ \mathbf{F}t^Y(\omega+i\gamma)t^X(-\omega-i\gamma)\} \tag{4}$$

The solution of the response equations yielding the amplitudes $t^Y(\omega+i\gamma)$ is discussed later in this section.

For the NEXAFS cross section, the imaginary part of the complex dipole-dipole polarizability in Eq. (4) is needed, which is obtained according to

$$\Im\langle\langle X;X\rangle\rangle_\omega^\gamma = \eta_\Re^X t_\Im^X(\omega+i\gamma)+\eta_\Re^X t_\Im^X(-\omega-i\gamma)+ \mathbf{F}t_\Im^X(\omega+i\gamma)t_\Re^X(-\omega-i\gamma)+\mathbf{F}t_\Im^X(-\omega-i\gamma)t_\Re^X(\omega+i\gamma) \tag{5}$$

where we have explicitly split the complex response amplitudes into real and imaginary parts

$$t^X(\omega+i\gamma) = t_\Re^X(\omega+i\gamma)+it_\Im^X(\omega+i\gamma) , \tag{6}$$

and made use of the relation

$$-t_\Im^X(-\omega+i\gamma) = t_\Im^X(-\omega-i\gamma) , \tag{7}$$

which is valid for all real operators (components) X. For an imaginary operator (component) χ, like the magnetic moment m, the latter relation reads

$$-t_\Re^\chi(-\omega+i\gamma) = t_\Re^\chi(-\omega-i\gamma) . \tag{8}$$

An imaginary operator is needed to compute the XCD cross section in Eq. (2), according to

$$\Re\langle\langle X;\chi\rangle\rangle_\omega^\gamma = \tfrac{1}{2}\Big(\eta_\Re^X t_\Re^\chi(\omega+i\gamma)-\eta_\Re^X t_\Re^\chi(-\omega-i\gamma) - \eta_\Im^\chi t_\Im^X(-\omega-i\gamma)+\eta_\Im^\chi t_\Im^X(\omega+i\gamma) + \mathbf{F}t_\Re^X(-\omega-i\gamma)t_\Re^\chi(\omega+i\gamma)-\mathbf{F}t_\Re^X(\omega+i\gamma)t_\Re^\chi(-\omega-i\gamma) - \mathbf{F}t_\Im^X(-\omega-i\gamma)t_\Im^\chi(\omega+i\gamma)+\mathbf{F}t_\Im^X(\omega+i\gamma)t_\Im^\chi(-\omega-i\gamma)\Big) \tag{9}$$

In the RIXS amplitudes, the operator X and Y are always real, and both real and imaginary components are needed. The general complex expressions of the KHD amplitudes within damped CC response theory (as well as EOM-CCSD) were presented in Ref.

9, and can be split into real and imaginary parts as given below for ${}^{\mathrm{CC}}\mathscr{F}^{f0}_{XY}(\omega)$:

$$\begin{aligned}
{}^{\mathrm{CC}}\mathscr{F}^{f0}_{XY}(\omega) = -L_f \Big[& \mathbf{A}^X t^Y_{\Re}(\omega+i\gamma) + \mathbf{A}^Y t^X_{\Re}(-\omega'-i\gamma) \\
& + \mathbf{B} t^Y_{\Re}(\omega+i\gamma) t^X_{\Re}(-\omega'-i\gamma) \\
& - \mathbf{B} t^Y_{\Im}(\omega+i\gamma) t^X_{\Im}(-\omega'-i\gamma) \Big] \\
-iL_f \Big[& \mathbf{A}^X t^Y_{\Im}(\omega+i\gamma) + \mathbf{A}^Y t^X_{\Im}(-\omega'-i\gamma) \\
& + \mathbf{B} t^Y_{\Re}(\omega+i\gamma) t^X_{\Im}(-\omega'-i\gamma) \\
& + \mathbf{B} t^Y_{\Im}(\omega+i\gamma) t^X_{\Re}(-\omega'-i\gamma) \Big]
\end{aligned} \tag{10}$$

A similar expression can be derived for ${}^{\mathrm{CC}}\mathscr{F}^{0f}_{XY}(\omega)$.

While referring to, e.g., Refs. 9,35 for a definition of the remaining CC building blocks in the expressions above, we return to the solution of the complex response equations needed to obtain the real and imaginary components of the complex amplitudes $t^X(\omega+i\gamma)$ and multipliers $\bar{t}^X(\omega-i\gamma)$:

$$(\mathbf{A} - (\omega+i\gamma)\mathbf{I}) t^X(\omega+i\gamma) = -\xi^X \tag{11}$$

$$\bar{t}^X(\omega'-i\gamma)(\mathbf{A} + (\omega'-i\gamma)\mathbf{I}) = -\eta^X - \mathbf{F} t^X(\omega'-i\gamma) \tag{12}$$

They can be recast in (pseudo-symmetric) matrix form like, e.g.

$$\begin{pmatrix} (\mathbf{A}-\omega\mathbf{I}) & \gamma\mathbf{I} \\ \gamma\mathbf{I} & -(\mathbf{A}-\omega\mathbf{I}) \end{pmatrix} \begin{pmatrix} t^X_{\Re} \\ t^X_{\Im} \end{pmatrix} = \begin{pmatrix} -\xi^X_{\Re} \\ \xi^X_{\Im} \end{pmatrix} \tag{13}$$

and solved via an iterative subspace algorithm as discussed in Refs. 14 and 9.

An important step to ensure convergence in the iterative algorithm is the generation of new trial vectors as

$$\widetilde{b_{n+1}} = \mathscr{P}\widetilde{R_{n+1}} \tag{14}$$

where $\widetilde{b_{n+1}}$ is a general new trial vector, $\widetilde{R_{n+1}}$ is a general residual in iteration n+1 and $\mathscr{P}$ is a preconditioner. In the iterative algorithm of Refs. 14 and 9, Eq. (14) is implemented as

$$\begin{aligned}
\begin{pmatrix} b_{\Re,n+1} \\ b_{\Im,n+1} \end{pmatrix} &= [(\mathbf{A}_0 - \omega\mathbf{I})^2 + \gamma^2\mathbf{I}]^{-1} \\
&\otimes \begin{pmatrix} (\mathbf{A}_0-\omega\mathbf{I}) & \gamma\mathbf{I} \\ \gamma\mathbf{I} & -(\mathbf{A}_0-\omega\mathbf{I}) \end{pmatrix} \begin{pmatrix} R_{\Re,n+1} \\ R_{\Im,n+1} \end{pmatrix}.
\end{aligned} \tag{15}$$

where $\mathbf{A}_0$ ia a diagonal approximation of the full Jacobian $\mathbf{A}$. A typical choice as $\mathbf{A}_0$ is to use the energy differences between virtual and occupied orbitals $\Delta\varepsilon_\mu$, where μ refers to a given excitation level. In the CCSD case, $(\varepsilon_a - \varepsilon_i)$ is used for the corresponding singles, and $(\varepsilon_a + \varepsilon_b - \varepsilon_i - \varepsilon_j)$ for the doubles.

Despite the preconditioner, and as anticipated in the introduction, the iterative subspace algorithm of Refs. 14 and and 9, does not converge at the CCSD level (in larger basis sets) when solving for the complex response amplitudes at positive values of ω falling in the x-region. The same occurs when solving for the response multipliers at negative frequencies in the x-region.. In the case of the CC2 method, on the other hand, the damped response equations always converge. The double-double block of the CC2 Jacobian matrix is exactly a diagonal matrix containing the orbital energy differences.

While a finite value of γ ensures that Eq. (13) will not be exactly singular for any value of ω, the solution of this equation becomes nonetheless unfeasible if many excitation energies are very close to ω. The X-ray region is beyond the (valence-)ionization limit of common molecules and there is therefore a continuum of ionized states near any given core-excitation energy. In calculations using finite basis sets, a discrete set of ionization energies is found and, for methods that only include single excitations, this set might be sparse enough not to prevent convergence of the damped response equations in the X-ray region. For models, such as CCSD, that explicit include double excitations, however, the set of ionized states is so dense that the normal damped response equations will not converge except for the smallest molecules and basis sets.

The problem of separating bound states from the continuum of ionized states can be solved using the CVS approximation,[26] which has recently been introduced in the context of CC theory to describe core-excited and core-ionized states.[27,31] In the present work, we propose to use a CVS projector in Eq. (13), whenever the frequency ω is positive and falls in the X-ray region.

This projector allows only the part of the CC amplitudes in Eq. (11) that involve core electrons to respond to the external electric field, effectively removing the valence ionization contribution. Similarly, a CVS projector is applied in the multiplier equation, Eq. (12), for negative ω'. In the opposite case, negative ω in Eq. (11) and positive ω' in Eq. (12), the equations are strongly diagonally dominant for absolute values of ω in the X-ray region and can easily be solved without applying projectors of any kind.

Comparing to the formulation of CVS-CCLR of Coriani and Koch,[27] projecting out the valence excitation space from the right and left response equations only for the above mentioned frequency values corresponds to projecting out exclusively from the eigenvalue equations. However, in Ref. 27, it was suggested one could apply CVS also to the left multipliers $\bar{M}_f$ equations, even though they are convergent. To obtain a damped-response CVS scheme equivalent to a CVS scheme where also the $\bar{M}_f$ equations are projected out, we would need to apply the CVS projector to all equations where the magnitude of the frequency is in the X-ray region, no matter its sign. Even though the effect of projecting out from the $\bar{M}_f$ vectors is negligible, our recommendation is however not to project them.

3 Results and Discussion

3.1 Computational details

For the illustrative results on water, the same geometry and basis set we adopted previously[9] was used. The geometry of acetone was optimized at the CCSD(T) level using the aug-cc-pVTZ basis set using CFOUR.[36] The structure of methyloxirane was optimized at the MP2/aug-cc-pCVTZ level also using CFOUR. In de-

termining the valence excited states for the RIXS calculations, the core orbitals have been kept frozen in the excited state calculation. The ground state parameters were optimized in full space. The same procedure was adopeted for the valence ionized states required to obtain the XES strengths.

3.2 NEXAFS and XCD

As illustration of cases that we could otherwise not tackle, due to convergence issues, with the full-space CPP solver in a basis set as large as 6-311++G**, we show, in Figs. 1 and 2, the CPP-CVS-XAS spectra of *S*-methyloxirane and acetone at the carbon K-edge, respectively, together with the XAS sticks obtained from a conventional linear response calculation using the CVS Davidson algorithm of Ref. 27. The XAS spectrum of methyloxirane has been measured by Piancastelli *et al.* [37] at both C and O K-edges, and by Turchini *et al.* [38] at the C K-edge. The XAS spectra of acetone have been measured by Prince *et al.* [39]

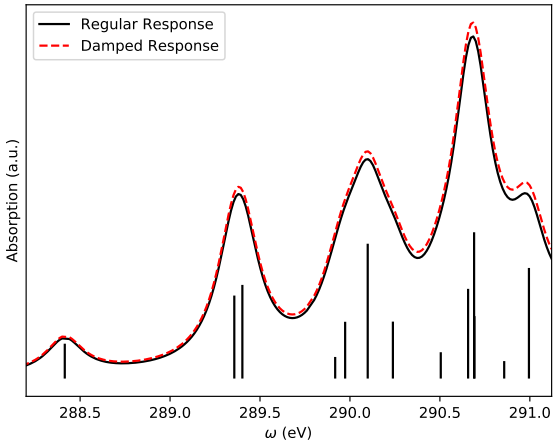

Fig. 1 CVS-CPP-CCSD results for the XAS spectrum of *S*-methyloxirane at the carbon K-edge in the 6-311++G** basis set, with underlying oscillator strengths obtained from standard CVS-CCSD calculations. The dashed red curve is the CVS-CPP result, whereas the black curve was obtained by applying a Lorentzian broadening to the CVS-CCSD sticks.

The XCD of methyloxirane has been experimentally measured by Turchini *et al.* [38] at the carbon K-edge. The study of Turchini *et al.* is the first (and only) CD measurement on a randomly oriented system and it was performed in vapour phase. Computational investigations have been presented at the random phase approximation level by Alagna *et al.*, [40] and using STEX by Carravetta *et al.* [41]

In Fig. 3, we compare the XCD spectrum of methyloxirane calculated using CVS-CPP-CCSD with the one obtained from a CVS-CCSD-LR calculation. The CPP-CVS-CCSD calculations were performed on a grid with a spacing of $5 \cdot 10^{-4}$ Hartree between points and with a broadening factor of 1000 cm^{-1}. Our calculated spectra present bands and sticks somewhat consistent with the computed spectral sticks of Ref. 41, whereas the agreement with the experimental spectrum is far from satisfactory. Further investigations are required to firmly assess the origin of the observed

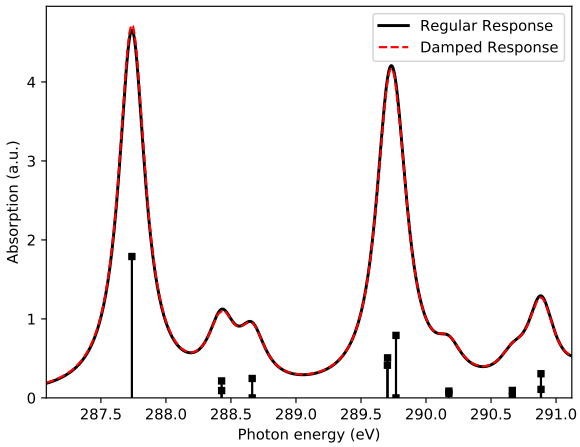

Fig. 2 CVS-CPP-CCSD results for the XAS spectrum of acetone at the carbon K-edge in the 6-311++G** basis set, with underlying oscillator strengths obtained from standard CVS-CCSD calculations. The dashed red curve is the CVS-CPP result, whereas the black curve was obtained by applying a Lorentzian broadening to the CVS-CCSD sticks.

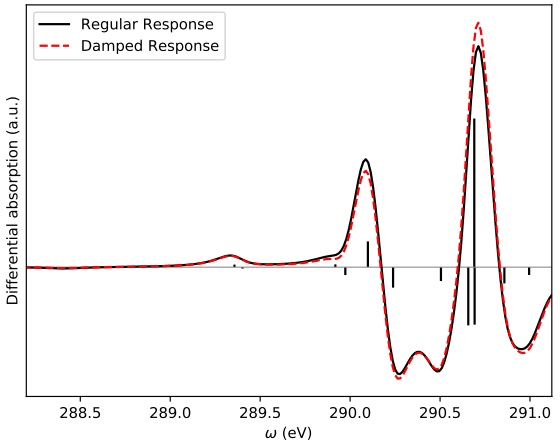

Fig. 3 CVS-CPP-CCSD results for the XCD spectrum of *S*-methyloxirane in the 6-311++G** basis set, with underlying rotatory strengths obtained from standard CVS-CCSD calculations. The dashed red curve is the CVS-CPP result whereas the black curve was obtained by applying a Lorentzian broadening to the CVS-CCSD sticks.

discrepancies.

3.3 RIXS and XES

Turning our attention to RIXS and non-resonant XES, we report in Fig. 4 a comparison of RIXS and XES spectral slices obtained with the here-proposed CVS-CPP approach, and with the full-space approach of Ref. 9 for water. As observed, the CVS projection introduces only a very modest shift of the peaks on the energy axis. The differences in intensities are also quite modest and the assignment of the origin of the spectral bands remains as previously done.[9] XES and RIXS spectra for water generated using the CVS-CPP solver and 40 valence excited states are shown in Fig. 5. The third relative intense band that is also experimentally observed emerges now at the resonant frequencies of the $1s\rightarrow 4a_1$ and $1s\rightarrow 2b_2$ core excitations. Even 40 valence excited states are, on the other hand, not sufficient to yield it when a resonant pump frequency close to the third XAS band is used. The third band is reproduced in the XES spectrum.

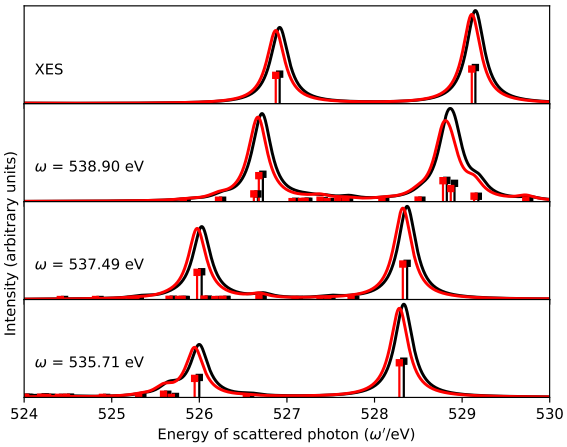

Fig. 4 Full-space CPP-CCSD (black) versus CVS-CPP-CCSD (red) results for the RIXS and XES spectra of water in the 6-311++G**+Ryd basis set.

As another example of the applicability of the CVS-CPP approach to RIXS, we considered the case of acetone at the oxygen K-edge. Despite the still moderate size of the molecule, its RIXS spectra could not be computed using the full-space CPP-CCSD approach, whereas they are easily obtained with the CVS-CPP solver. Table 1 collects the excitation energies and strengths of the valence excited states that have been considered in the spectral simulation. The resonant pump frequency was chosen at the value of the first core excitation at the oxygen K-edge, see also Table 2. The computed RIXS and XES spectral slices are shown in Fig. 6. Experimental resonant (RIXS) and non-resonant (XES) spectral slices at the oxygen K-edge in solution were available from Ref. 42, see also Ref. 43. The re-digitized experimental curves have been overlapped to the computed spectra without any shift on the energy axis. Despite the misalignment, the main spectral features at the lower core excitation in the resonant RIXS spectrum, as well as the XES spectrum, are reproduced. As it can be appreci-

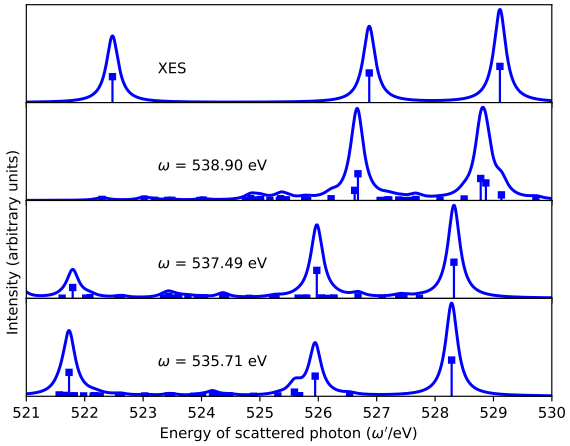

Fig. 5 CVS-CPP-CCSD results for the RIXS and XES (panel labeled 'non-resonant') spectra of water in the 6-311++G**+Ryd basis set including the third peak, generated using 40 valence excited states.

Table 1 The valence excitation energies (ω_n), transition (S_{n0}) and oscillator (f_{n0}) strengths of acetone as calculated at the CCSD/6-311++G** level.

Symmetry	ω_n (a.u.)	ω_n (eV)	S_{n0} (a.u.)	f_{n0}
A_2	0.166849	4.5402	0.0000000	0.00000
B_2	0.238143	6.4802	0.1991480	0.03162
A_1	0.278881	7.5887	0.0000052	0.00000
A_2	0.279308	7.6003	0.0000000	0.00000
B_2	0.286427	7.7941	0.0479960	0.00916
B_2	0.300078	8.1655	0.1921846	0.03845
A_1	0.309681	8.4269	0.3608999	0.07451
B_1	0.321666	8.7530	0.0891817	0.01912
B_2	0.325418	8.8551	0.0069247	0.00150
A_2	0.329077	8.9546	0.0000000	0.00000
B_1	0.345325	9.3968	0.0219041	0.00504
B_1	0.346340	9.4244	0.0315136	0.00728
A_1	0.346448	9.4273	1.3455875	0.31078
B_2	0.346749	9.4355	0.0759524	0.01756
A_2	0.354554	9.6479	0.0000000	0.00000
B_1	0.364546	9.9198	0.0042734	0.00104
A_1	0.365335	9.9413	0.0096702	0.00235
B_2	0.375621	10.221	0.1865032	0.04670
B_2	0.378524	10.300	0.1435405	0.03622
A_2	0.381769	10.388	0.0000000	0.00000
A_1	0.387199	10.536	0.0279431	0.00721
A_2	0.388462	10.571	0.0000000	0.00000
A_1	0.389988	10.612	0.1629636	0.04237
B_1	0.397173	10.808	0.2212859	0.05859
A_1	0.398122	10.833	0.4069430	0.10801
A_2	0.404636	11.012	0.0000000	0.00000
B_2	0.405736	11.041	0.3600519	0.09739
B_1	0.408028	11.103	0.0198221	0.00539
A_1	0.412197	11.216	0.1073709	0.02950
B_2	0.415604	11.309	0.2804371	0.07770

Table 2 Oxygen K-edge excitation energies (ω_n), transition (S_{n0}) and oscillator (f_{n0}) strengths of acetone as calculated at the CVS-CCSD/6-311++G** level.

ω_n (a.u.)	ω_n (eV)	S_{n0} (a.u.)	f_{n0}
19.5892	533.05	0.0033221	0.04338
19.7441	537.26	0.0000000	0.00000
19.7855	538.39	0.0001939	0.00256
19.7880	538.46	0.0000809	0.00107
19.7910	538.54	0.0001268	0.00167
19.8098	539.05	0.0000418	0.00055

ated from Fig. 6, the overall shift of the XES spectrum is slightly larger than for the RIXS one, an indication that CCSD describes relaxation effects on XES (or, at leas, on XES as computed here[9] at CCSD level) less accurately than those on RIXS.

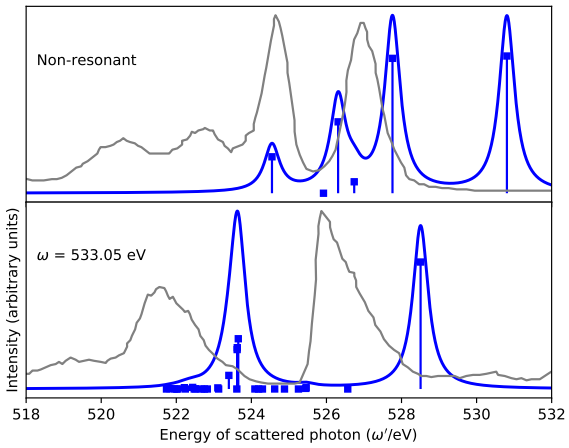

Fig. 6 CVS-CPP-CCSD results for the RIXS (bottom panel) and XES (upper panel) spectra at the Oxygen K-edge of acetone in the 6-311++G** basis set. The experimental spectral slices in solution from Ref. 42 are also shown. Note that the computed spectra have not been shifted to align to the experimental ones.

4 Conclusions

We have presented a core-valence separated strategy to solve the complex response equations of coupled cluster damped response theory at the singles and doubles level. Introducing the CVS at specific values of the external frequency allows to overcome convergence problems that appear in the CCSD case due to the continuum of valence ionized states. The modified solver has been used to compute XAS, XCD, RIXS and XES spectra of selected molecules, showing moderate shifts of the peak positions and intensities compared to the cases where full-space calculations could be performed.

Conflicts of interest

There are no conflicts of interest to declare.

Acknowledgements

We thank K. Nanda and Anna I. Krylov for useful discussions. We acknowledge support from DTU Chemistry and from the Independent Research Fund Denmark – DFF-Forskningsprojekt2 grant no. 7014-00258B.

References

1 P. Norman, D. M. Bishop, H. J. A. Jensen and J. Oddershede, *J. Chem. Phys.*, 2001, **115**, 10323–10334.
2 P. Norman, D. Bishop, H. J. A. Jensen and J. Oddershede, *J. Chem. Phys.*, 2005, **123**, 194103.
3 L. Jensen, J. Autschbach and G. C. Schatz, *J. Chem. Phys.*, 2005, **122**, year.
4 U. Ekström, P. Norman, V. Carravetta and H. Ågren, *Phys. Rev. Lett.*, 2006, **97**, 143001.
5 U. Ekström and P. Norman, *Phys. Rev. A*, 2006, **74**, 042722.
6 T. Fahleson, H. Ågren and P. Norman, *J. Phys. Chem. Lett.*, 2016, **7**, 1991–1995.
7 S. Coriani, T. Fransson, O. Christiansen and P. Norman, *J. Chem. Theory Comput.*, 2012, **8**, 1616–1628.
8 S. Coriani, O. Christiansen, T. Fransson and P. Norman, *Phys. Rev. A*, 2012, **85**, 022507.
9 R. Faber and S. Coriani, *J. Chem. Theory Comput.*, 2019, **15**, 520–528.
10 P. Norman, *Phys. Chem. Chem. Phys.*, 2011, **13**, 20519–20535.
11 K. Kristensen, J. Kauczor, T. Kjaergaard and P. Jørgensen, *J. Chem. Phys.*, 2009, **131**, 044112.
12 J. Kauczor and P. Norman, *J. Chem. Theory Comput.*, 2014, **10**, 2449–2455.
13 T. Fransson, D. R. Rehn, A. Dreuw and P. Norman, *J. Chem. Phys.*, 2017, **146**, 094301.
14 J. Kauczor, P. Norman, O. Christiansen and S. Coriani, *J. Chem. Phys.*, 2013, **139**, 211102.
15 P. Reinholdt, M. S. Nørby and J. Kongsted, *J. Chem. Theory Comput.*, 2018, **14**, 6391–6404.
16 M. Nørby, S. Coriani and J. Kongsted, *Theor. Chem. Acc.*, 2018, **137**, year.
17 T. Fransson, D. Burdakova and P. Norman, *Phys. Chem. Chem. Phys.*, 2016, **18**, 13591–13603.
18 A. Jiemchooroj and P. Norman, *J. Chem. Phys.*, 2007, **126**, 134102.
19 H. Solheim, K. Ruud, S. Coriani and P. Norman, *J Chem. Phys.*, 2008, **128**, 094103.
20 T. Fahleson, J. Kauczor, P. Norman, F. Santoro, R. Improta and S. Coriani, *J. Phys. Chem. A*, 2015, **119**, 5476–5489.
21 J. Vaara, A. Rizzo, J. Kauczor, P. Norman and S. Coriani, *J. Chem. Phys.*, 2014, **140**, 134103.
22 J. Cukras, J. Kauczor, P. Norman, A. Rizzo, G. L. J. A. Rikken and S. Coriani, *Phys. Chem. Chem. Phys.*, 2016, **18**, 13267–13279.
23 K. Kristensen, J. Kauczor, A. J. Thorvaldsen, P. Jørgensen, T. Kjærgaard and A. Rizzo, *J. Chem. Phys.*, 2011, **134**, 214104.
24 A. Jiemchooroj, B. E. Sernelius and P. Norman, *Phys. Rev. A*, 2004, **69**, 044701.
25 D. R. Rehn, A. Dreuw and P. Norman, *J. Chem. Theory Comput.*, 2017, **13**, 5552–5559.
26 L. S. Cederbaum, W. Domcke and J. Schirmer, *Phys. Rev. A: At. Mol. Opt. Phys.*, 1980, **22**, 206–222.
27 S. Coriani and H. Koch, *J. Chem. Phys.*, 2015, **143**, 181103.
28 B. N. C. Tenorio, T. Moitra, M. A. C. Nascimento, A. B. Rocha and S. Coriani, *J. Chem. Phys.*, 2019, **150**, 224104.
29 F. Pawłowski, J. Olsen and P. Jørgensen, *J. Chem. Phys.*, 2015, **142**, 114109.
30 S. Coriani, F. Pawłowski, J. Olsen and P. Jørgensen, *J. Chem. Phys.*, 2016, **144**, 024102.

31 M. L. Vidal, X. Feng, E. Epifanovsky, A. I. Krylov and S. Coriani, *J. Chem. Theory Comput.*, 2019, **15**, 3117–3133.

32 K. Nanda, M. L. Vidal, R. Faber, S. Coriani and A. I. Krylov, *Phys. Chem. Chem. Phys.*, 2019.

33 F. Gel'mukhanov and H. Ågren, *Phys. Rep.*, 1999, **312**, 87–330.

34 D. A. Long, *The Raman Effect: A Unified Treatment of the Theory of Raman Scattering by Molecules*, John Wiley & Sons Ltd., 2002.

35 O. Christiansen, P. Jørgensen and C. Hättig, *Int. J. Quantum Chem.*, 1998, **68**, 1–52.

36 J. F. Stanton, J. Gauss, L. Cheng, M. E. Harding, D. A. Matthews and P. G. Szalay, *CFOUR, Coupled-Cluster techniques for Computational Chemistry, a quantum-chemical program package*, With contributions from A.A. Auer, R.J. Bartlett, U. Benedikt, C. Berger, D.E. Bernholdt, Y.J. Bomble, O. Christiansen, F. Engel, R. Faber, M. Heckert, O. Heun, M. Hilgenberg, C. Huber, T.-C. Jagau, D. Jonsson, J. Jusélius, T. Kirsch, K. Klein, W.J. Lauderdale, F. Lipparini, T. Metzroth, L.A. Mück, D.P. O'Neill, D.R. Price, E. Prochnow, C. Puzzarini, K. Ruud, F. Schiffmann, W. Schwalbach, C. Simmons, S. Stopkowicz, A. Tajti, J. Vázquez, F. Wang, J.D. Watts and the integral packages MOLECULE (J. Almlöf and P.R. Taylor), PROPS (P.R. Taylor), ABACUS (T. Helgaker, H.J. Aa. Jensen, P. Jørgensen, and J. Olsen), and ECP routines by A. V. Mitin and C. van Wüllen. For the current version, see http://www.cfour.de.

37 M. Piancastelli, T. Lischke, G. Prümper, X. Liu, H. Fukuzawa, M. Hoshino, T. Tanaka, H. Tanaka, J. Harries, Y. Tamenori, Z. Bao, O. Travnikova, D. Céolin and K. Ueda, *J. Electron Spectr. Rel. Phenom.*, 2007, **156-158**, 259 – 264.

38 S. Turchini, N. Zema, S. Zennaro, L. Alagna, B. Stewart, R. D. Peacock and T. Prosperi, *J. Am. Chem. Soc.*, 2004, **126**, 4532–4533.

39 K. C. Prince, R. Richter, M. de Simone, M. Alagia and M. Coreno, *J. Phys. Chem. A*, 2003, **107**, 1955–1963.

40 L. Alagna, S. D. Fonzo, T. Prosperi, S. Turchini, P. Lazzeretti, M. Malagoli, R. Zanasi, C. Natoli and P. Stephens, *Chemical Physics Letters*, 1994, **223**, 402 – 410.

41 V. Carravetta, O. Plachkevytch, O. Vahtras and H. ÃĚgren, *Chemical Physics Letters*, 1997, **275**, 70 – 78.

42 K. M. Lange and E. F. Aziz, *Chem. Soc. Rev.*, 2013, **42**, 6840–6859.

43 K. Atak, N. Engel, K. M. Lange, R. Golnak, M. Gotz, M. Soldatov, J.-E. Rubensson, N. Kosugi and E. F. Aziz, *ChemPhysChem*, 2012, **13**, 3106–3111.